

Sensitivity of large-footprint lidar to canopy structure and biomass in a neotropical rainforest

Jason B. Drake^{a,*}, Ralph O. Dubayah^a, Robert G. Knox^b, David B. Clark^{c,d}, J.B. Blair^e

^aDepartment of Geography, University of Maryland, College Park, MD 20742, USA

^bBiospheric Sciences Branch, NASA's Goddard Space Flight Center, Greenbelt, MD 20771, USA

^cDepartment of Biology, University of Missouri-St. Louis, St. Louis, MO 63121, USA

^dLa Selva Biological Station, Puerto Viejo de Sarapiquí Costa Rica

^eLaser Remote Sensing Branch, Laboratory for Terrestrial Physics, NASA Goddard Space Flight Center, Greenbelt, MD 20771, USA

Received 20 June 2001; received in revised form 25 January 2002; accepted 29 January 2002

Abstract

Accurate estimates of the total biomass in terrestrial vegetation are important for carbon dynamics studies at a variety of scales. Although aboveground biomass is difficult to quantify over large areas using traditional techniques, lidar remote sensing holds great promise for biomass estimation because it directly measures components of canopy structure such as canopy height and the vertical distribution of intercepted canopy surfaces. In this study, our primary goal was to explore the sensitivity of lidar to differences in canopy structure and aboveground biomass in a dense, neotropical rainforest. We first examined the relationship between simple vertical canopy profiles derived from field measurements and the estimated aboveground biomass (EAGB) across a range of field plots located in primary and secondary tropical rainforest and in agroforestry areas. We found that metrics from field-derived vertical canopy profiles are highly correlated (R^2 up to .94) with EAGB across the entire range of conditions sampled. Next, we found that vertical canopy profiles from a large-footprint lidar instrument were closely related with coincident field profiles, and that metrics from both field and lidar profiles are highly correlated. As a result, metrics from lidar profiles are also highly correlated (R^2 up to .94) with EAGB across this neotropical landscape. These results help to explain the nature of the relationship between lidar data and EAGB, and also lay the foundation to explore the generality of the relationship between vertical canopy profiles and biomass in other tropical regions. © 2002 Elsevier Science Inc. All rights reserved.

1. Introduction

The total biomass of terrestrial vegetation is an important variable for studies at multiple scales. As biomass (i.e., the total over-dried biological material or mass in a given area at a given time) is approximately 50% carbon, changes in the total biomass through time are important from local (e.g., forest carbon dynamics) to global scales (e.g., carbon release from large forest fires). Because tropical areas contain a large proportion of the total carbon in terrestrial vegetation globally (Dixon et al., 1994), knowledge of the biomass content in tropical ecosystems can provide an initial condition or baseline for studies that examine carbon flux related to natural (e.g., disturbances) and anthropogenic (e.g., deforestation) processes. However, the estimation of

terrestrial vegetation biomass, especially in dense tropical forests, has proven difficult.

Most remote sensing techniques to estimate biomass are empirical, and illustrate the correlation between biomass and the intensity of electromagnetic radiation (or the ratio of energy at different wavelengths) that is received by the instrument (e.g., Steininger, 2000). In some cases, a modeling approach is also incorporated to explain the physical interaction between the electromagnetic radiation and forest canopy structure (e.g., Strahler, 1997). Many remote sensing instruments, however, have the same problem: they are able to detect differences in biomass in relatively young and/or homogeneous forests, but are not as sensitive to changes in biomass in older or heterogeneous forests (Imhoff, 1995; Waring et al., 1995; Weishampel, Ranson, & Harding, 1996; Wickland, 1991). As a result, estimating terrestrial biomass, especially in dense primary tropical forests has proven difficult (e.g., Curran, Foody, Lucas, Honzak, & Grace, 1997; Foody, Palubin-

* Corresponding author. Tel.: +1-301-405-4538; fax: +1-301-405-8662.
E-mail address: jasdrak@geog.umd.edu (J.B. Drake).

skas, Lucas, Curran, & Honzak, 1996; Luckman, Baker, Kuplich, Yanasse, & Frery, 1997; Moran, Brondizio, Mausel, & Wu, 1994; Sader, Waide, Lawrence, & Joyce, 1989; Steininger, 2000).

Light detecting and ranging (lidar) remote sensing is a relatively new active remote sensing technique with potential for estimation of terrestrial vegetation biomass (Drake et al., 2002; Dubayah & Drake, 2000; Dubayah, Knox, Hofton, Blair, & Drake, 2000; Lefsky, Cohen et al., 1999; Means et al., 1999). Lidar instruments have been used to accurately estimate canopy height (Drake & Weishampel, 2000; Lefsky, Harding, Cohen, Parker, & Shugart, 1999; Magnussen, Eggermont, & LaRicca, 1999; Nelson, Swift, & Krabill, 1988; Peterson, 2000) and vertical structure (Harding, Lefsky, Parker, & Blair, 2001; Parker, Lefsky, & Harding, 2001) in a variety of different forest types. As a result, lidar instruments reliably provide important biophysical characteristics that can then be used to estimate changes in biomass in forests.

The empirical relationships between lidar-derived canopy height and forest biomass are conceptually similar to the allometric relationships used in field studies (Niklas, 1994). The primary difference is that instead of relating changes in the height or diameter of individual trees to the changes in biomass, the relationship is between lidar-derived canopy height (or other lidar metrics) and the total aboveground biomass of all trees within the area of interest (e.g., a field plot). The changes in canopy height and structure through succession are also affected by ecological processes (e.g., competition, stand-thinning) operating on individual trees through time. The net result is that the vertical growth of forest stands also correlates with an overall increase in stand biomass levels.

In addition to canopy height, new large-footprint, full-digitization lidar instruments also provide data related to the vertical arrangement of forest structure from the top of the canopy to the ground (Dubayah et al., 1997; Dubayah & Drake, 2000; Dubayah et al., 2000; Harding et al., 2001). This data can also be used to improve the prediction of biomass (Drake et al., 2002; Lefsky, Cohen et al., 1999; Lefsky, Harding et al., 1999; Means et al., 1999), and to estimate the vertical distribution of forest structure such as vertical foliar profiles (Harding et al., 2001) and the vertical distribution of light transmittance (Parker et al., 2001). As such, lidar instruments provide a wealth of data potentially suited for estimation of biomass in carbon-rich tropical forest ecosystems.

Drake et al. 2002 showed that metrics from an airborne large-footprint lidar instrument were correlated with the estimated aboveground biomass (EAGB) across a successional spectrum of sites ranging from abandoned pasture to dense primary tropical forest. However, there is still a need to examine the nature of this empirical relationship to understand why metrics from lidar data are highly correlated with aboveground biomass in tropical forests. The generality of these relationships will bear on global applications of

these types of lidar data such as the vegetation canopy lidar (VCL) mission (Dubayah et al., 1997) and on the design of future lidar instruments.

The primary goal of this study is to explore the sensitivity of lidar to vertical canopy structure and biomass across a neotropical rainforest landscape. We hypothesize that the strong relationship between metrics from large-footprint, full-digitization lidar instruments and aboveground biomass in tropical forests is the result of: (1) the sensitivity of lidar to differences in vertical canopy structure and (2) the correlation between vertical canopy structure and total aboveground biomass. In both cases, the relationships may be valid across a wide range of successional and environmental conditions. To test these assertions, we take a three-step approach.

First, we examine the relationship between field-derived vertical canopy profiles and biomass. Metrics from the distributions of stem heights (e.g., maximum stem height) and from vertical canopy profiles derived from field measurements in a series of plots located in a dense tropical rainforest are compared to the total biomass in the plot. This approach reveals which components of vertical canopy structure are most correlated with total biomass across different successional (e.g., secondary vs. primary forest) and environmental (e.g., edaphic) conditions. In addition, the field-derived vertical canopy profile comparisons serve as a baseline with which to compare lidar-derived vertical canopy profiles. A key question we address is: are metrics from a vertical canopy profile correlated with aboveground biomass over the entire range of conditions encountered in a dense tropical rainforest, or do they saturate in old-growth or “primary” forest areas?

Second, we examine the relationship between vertical canopy profiles derived from both lidar and field techniques. Because of obscuration effects, less lidar energy is available at the bottom of the canopy, therefore, an existing transformation technique (Harding et al., 2001; Lefsky, Harding et al., 1999) is also used on the lidar data for comparison. Metrics from both normal and transformed lidar profiles are then compared with corresponding metrics from field profiles. Next, we examine the relationship between complete profiles from lidar (normal and transformed) and field techniques. This process illustrates the relationship between vertical canopy profiles derived using vastly different techniques (i.e., field vs. lidar remote sensing), and whether transformations of lidar profiles are necessary. The two questions we address here are: (1) are metrics from untransformed or transformed lidar profiles correlated with metrics from field profiles and (2) are lidar- and field-derived vertical canopy profiles from each plot related or are they significantly different?

Finally, we compare the relationships between aboveground biomass and metrics from both field- and lidar-derived vertical canopy profiles. In this section, we illustrate how lidar compares with the field techniques for predicting aboveground biomass across different successional and

environmental conditions. The primary question in this section is: do metrics from lidar profiles explain the same level of variation in biomass as metrics from field profiles?

2. Methods

2.1. La Selva Biological Station

This study uses field and lidar data acquired at the La Selva Biological Station (McDade, Bawa, Hespdenheide, & Hartshorn, 1994), a 1536-ha tropical forest research facility located in northeast Costa Rica (Fig. 1). La Selva is comprised of a mixture of lowland primary and secondary tropical rainforest (classified as “tropical wet forest” in Holdridge, Grenke, Hatheway, Liang, & Tosi, 1971), agroforestry and plantation plots, and recently abandoned pastures (Matlock & Hartshorn, 1999; McDade et al., 1994). Within these separate areas, there are ongoing studies related to forest carbon dynamics (Clark & Clark, 2000), light environments in primary and secondary forests (Nicotra, Chazdon, & Iriarte, 1999), and the growth of commercially valuable trees in managed agroforestry plots (Menalled, Kelty, & Ewel, 1998), among many others.

2.2. Field data

Field data were collected across a wide range of successional, land-use and environmental conditions at La Selva (Fig. 1). Data were collected both as a part of the March 1998 prelaunch validation/calibration campaign of the VCL mission (Dubayah et al., 1997; Dubayah et al., 2000), and as a part of ongoing field studies at La Selva. Data from 3

different landcover types, 18 primary forest, 3 secondary forest, and 6 agroforestry plots were used in this study.

The 18 primary forest plots (0.5 ha each) are evenly stratified over three edaphic and topographic conditions: 6 are located in relatively fertile flat inceptisol areas on old alluvial terraces, six are in relatively infertile ultisol areas on ridgetops and six are in ultisol areas on steep slopes. All of these plot locations were identified in the laboratory using a GIS, and were established in the field without reference to surrounding forest conditions (i.e., their positions are not biased by local structural characteristics). In all primary plots, detailed measurements of stem diameters of all trees greater than 10 cm diameter have been collected annually as a part of ongoing carbon dynamics studies (see Clark & Clark, 2000 for more details). Stem diameters were measured either at breast height (1.37 m) or, when necessary, above buttressing.

Data in secondary forests were collected in three different areas that were approximately 14, 22 (Chazdon, 1996; Guariguata, Chazdon, Denslow, Dupuy, & Anderson, 1997; Nicotra et al., 1999), and 31 (Pierce, 1992) years old, respectively, as of March 1998. The 14- and 22-year-old secondary forest plots are each 0.5 ha. Six 25-m diameter circular plots were also geolocated to approximately coincide with lidar footprint locations within the 31-year-old secondary forest area. Within the 14- and 22-year-old secondary forest plots, all stem diameters greater than 5 cm diameter were measured. In the 31-year-old plot, all stem diameters greater than 10 cm diameter were measured. Because of the smaller size of the plots in the 31-year-old forest area, the field data from these six plots were pooled to form plot-level profiles (see below) and a single biomass estimate for this 31-year-old area.

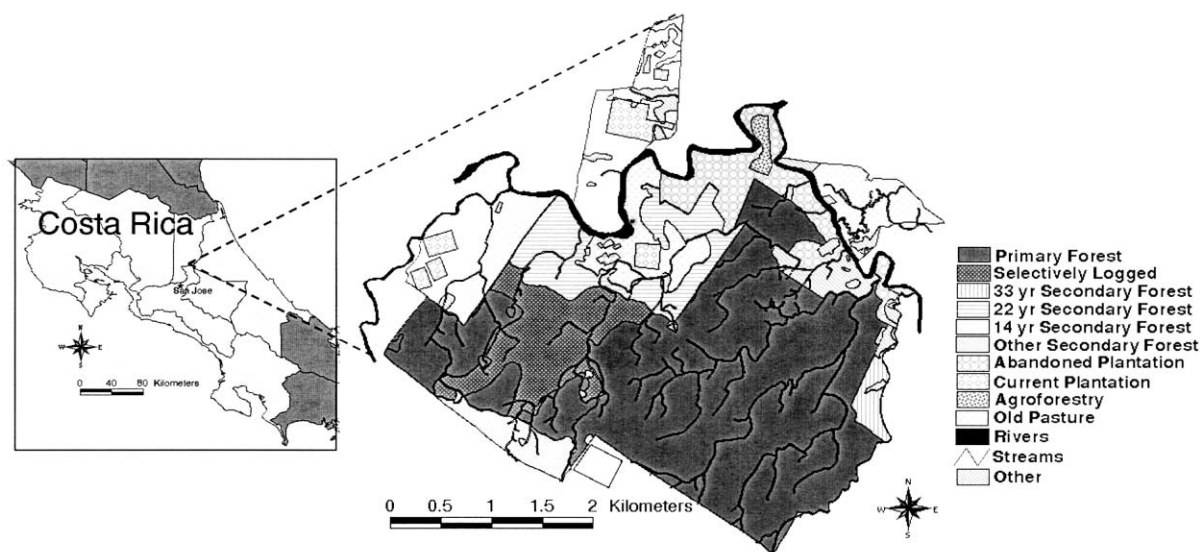


Fig. 1. Locator map for study site at La Selva Biological Station in northeastern Costa Rica. La Selva is a 1546-ha area comprised of a mixture of primary and secondary tropical rainforest, agroforestry, plantations, and recently abandoned pastures.

EAGB values were then calculated for all live stems in each forest plot using Eq. (1), which was developed for tropical wet forests (Brown, 1997). Plot-level EAGB values (in Mg/ha) were calculated by summing the EAGB values for all live stems within the plot.

$$\text{EAGB}_s = 21.297 - 6.953(D) + 0.740(D^2) \quad (1)$$

where D is stem diameter in centimeters and EAGB_s is the estimated oven-dried aboveground biomass (in kilogram) for the stem. Note that this equation relies exclusively on stem diameter and does not include tree height.

Within each plot, measurements related to vertical canopy structure were also collected on a subset of the trees, with a particular emphasis placed on canopy-forming trees (i.e., classified as either dominant or codominant). Stem heights and crown depths (i.e., from the top of the tree to the lowest live branch) were measured using a laser rangefinder. A reflector at the base of the tree was used as a target for horizontal distance measurements. Crown diameters were measured using either a laser rangefinder or standard fiberglass measuring tapes. The crown diameters were measured in the direction of the longest branches and, therefore, represent the maximum horizontal crown extent.

Stem diameter measurements were also used to estimate height and crown dimensions for all remaining trees where these measurements were not taken. Allometric relationships were developed to estimate stem height, crown diameter, and crown depth using the subset of trees sampled in each area (Table 1). Separate equations were developed for plots in secondary forest areas, and for plots located in primary forest areas with different edaphic conditions (inceptisol vs. ultisols). Separate equations compensated

Table 1
Regression models developed from stems with measured heights, crown depths, and crown diameter

Y	Plots	Equation	R^2	RMSE (m)
Height	Primary inceptisol ($n = 111$)	$y = 15.21 \ln(x) - 26.38$.822	3.6
	Primary ultisol ($n = 302$)	$y = 10.10 \ln(x) - 12.41$.483	5.1
	Secondary ($n = 631$)	$y = 10.77 \ln(x) - 11.63$.745	3.9
Crown depth	Primary inceptisol ($n = 111$)	$y = 0.306x + 1.24$.576	4.3
	Primary ultisol ($n = 302$)	$y = 0.16x + 3.76$.274	3.2
	Secondary ($n = 631$)	$y = 0.28x + 2.29$.495	3.0
Crown diameter	Primary inceptisol ($n = 111$)	$y = 0.20x + 4.17$.706	2.1
	Primary ultisol ($n = 302$)	$y = 0.14x + 4.41$.276	2.8
	Secondary ($n = 631$)	$y = 0.19x + 2.37$.532	1.9

Separate equations were developed for stems found in plots in secondary forests and in primary forest areas with different soil conditions. For all equations, x = stem diameter (cm).

for differences in the coefficient of variation of height and crown measurements in each area that may have been the result of different field crews in each respective area.

Finally, published aboveground biomass and crown volume values from six (0.12 ha) agroforestry plots at La Selva (Menalled et al., 1998) were incorporated into this study. The approximate locations of these plots were determined using an ancillary fine-resolution (~ 33 cm) lidar data set collected over the northern portion of La Selva (Roth, unpublished; Blair & Hofton, 1999).

2.3. Derivation of field vertical canopy profiles

Vertical canopy profiles were derived from measured and modeled stem heights and crown dimensions in all plots. The field-derived vertical canopy profiles are comprised of a total of one hundred eighty 30-cm bins (to correspond with the vertical bin size of the lidar waveforms), for a total height of 54 m. The profiles represent the vertical distribution of crown volume, and the methods for deriving them are described next.

First, all crowns are modeled to have a simple cylindrical shape bounded by the crown depth and crown diameter values, and placed at the appropriate height according to the stem height value. Second, the total cross-sectional area of all intersected crowns within each 30-cm vertical bin is then summed. For each plot, this produces a vertical canopy profile based on the distribution of crown volume. This process is illustrated in Fig. 2.

Quantile metrics are then calculated for each average profile to represent the relative distribution of canopy materials within each plot (Fig. 2). These metrics represent the height below which X of the total crown volume is located (denoted as FCVX, where X represents the percentage of “FCV” or field-estimated crown volume). For this study, FCV01, FCV05, FCV10, FCV25, FCV75, FCV90, FCV95, FCV99, and “HMFCV” (the height of median crown volume, equivalent to FCV50) were calculated. For simplicity, not all metrics are shown in Section 3.

2.4. Lidar data

The lidar data used in this study are from the airborne Laser Vegetation Imaging Sensor (LVIS; Blair, Rabine, & Hofton, 1999). LVIS is a medium-altitude, medium-to large-footprint imaging laser altimeter, designed and developed at NASA’s Goddard Space Flight Center. LVIS digitizes the entire return signal, thus, providing a waveform relating to the vertical distribution of intercepted canopy and ground surfaces within each footprint (Fig. 3) (see Blair et al., 1999; Dubayah & Drake, 2000; Dubayah et al., 2000 for more details).

In March 1998, LVIS was flown in a NASA C-130 cargo plane over La Selva Biological Station and surrounding regions of northeast Costa Rica. LVIS was flown at an altitude of 8 km above the ground to produce eighty, 25-m

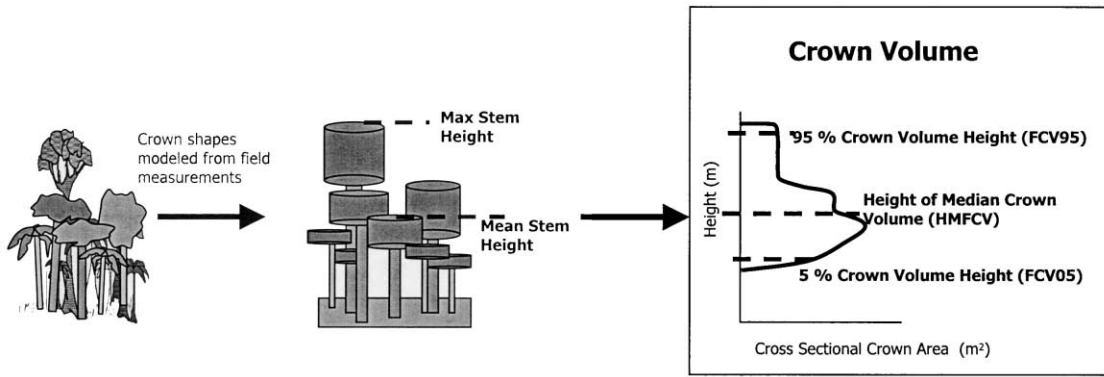


Fig. 2. Derivation of field vertical canopy profiles. For this study, crown volume distributions were calculated from field measurements in all plots. A simple cylindrical crown shape, bounded by crown depth and crown diameter measurements, was assumed for tree crowns. The cross-sectional area of all crowns intersected is then summed for each 30-cm height interval. Metrics were derived from both the distribution of tree heights (e.g., mean stem height) and from the vertical canopy profiles (e.g., FCV95).

diameter footprints separated by ~ 25 m along- and ~ 9 m across-track. Only LVIS footprints that were coincident with field study plots were selected for this study. The mean number of LVIS footprints in each plot was approximately eight.

2.5. Lidar-derived vertical canopy profiles

The signal digitized by LVIS is a waveform that relates to the vertical distribution of intercepted canopy and ground surfaces (in 30-cm vertical bins). As such, LVIS waveforms from within each plot were used as one type of vertical canopy profile. In this case, all of the lidar waveforms within a plot were summed to produce a plot-level “average waveform” with which to compare to field-derived vertical canopy profiles from each plot.

Lidar waveforms have also been transformed in previous studies to account for the attenuation of the lidar energy as the laser pulse travels through the canopy (Harding et al., 2001; Lefsky, 1997; Lefsky, Cohen et al., 1999; Lefsky, Harding et al., 1999; Means et al., 1999). Because some of the laser energy at the top of the canopy is reflected or

absorbed, there will be less energy available lower into the canopy. Thus, the MacArthur–Horn technique (Aber, 1979b; MacArthur & Horn, 1969), which was developed for field studies to produce foliar height profiles from uplooking foliar distance measurements, was modified to transform the waveform into a relative canopy height profile (CHP) (Fig. 3) (see Harding et al., 2001 for more details).

CHPs were then calculated for all shots in each plot based on techniques described in Harding et al. (2001). In this case, the CHPs were created with one hundred eighty 30-cm bins. Plot-level CHPs were derived by summing all individual CHPs within each plot.

Quantile metrics were then calculated for each average lidar profile similar to the technique described above for field profiles (Fig. 3). The metrics represent the height below which $X\%$ of: (a) the total energy of the waveform (including the canopy and ground returns), or (b) the CHP are located. In this case, the denotations are: “HENGX” for the height at which $X\%$ of the waveform energy is located below and “CHPX” for the height at which $X\%$ of the CHP is located below. For this study, the 1, 5, 10, 25, 50, 75, 90, 95, and 99 quantile metrics were calculated for each type

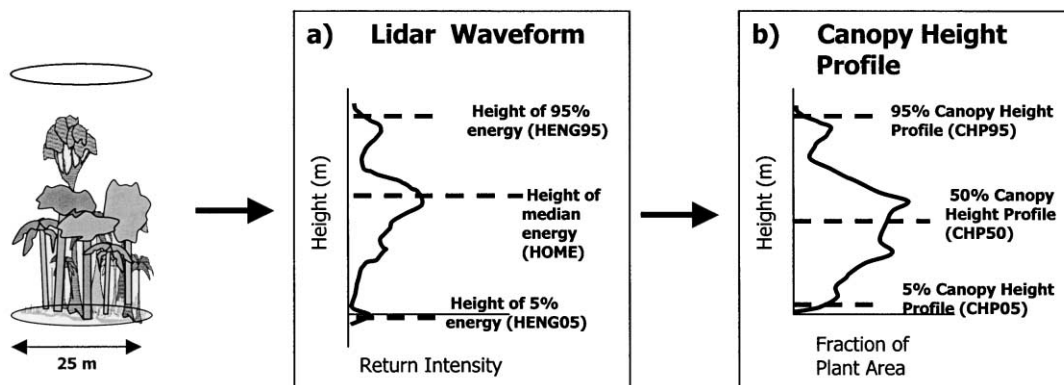


Fig. 3. Derivation of vertical canopy profiles from lidar data. Coincident footprints from each plot were used both as: (a) waveforms directly from the LVIS instrument and (b) canopy height profiles that are derived using an exponential transformation of return energy in the waveform as described in Harding et al. (2001). Quantiles (e.g., HOME, CHP50) were calculated from both lidar vertical canopy profile formats.

of lidar profile. The only exception to the above naming scheme is for the height of 50% of the waveform energy, which is referred to as the height of median energy (HOME) to correspond to a previous study (Drake et al., 2002). Again, for simplicity, not all metrics are shown in Section 3.

2.6. Analysis

We first examined the relationship between metrics from field-derived vertical canopy profiles and the EAGB. Profile metrics, along with the mean and maximum stem heights, for each plot were incorporated into a stepwise regression procedure to predict EAGB. The best single- and multiple-term relationships were identified. These relationships were also used as a baseline for comparisons against the lidar-EAGB relationships.

To compare field- and lidar-derived vertical canopy profiles, we first examined the relationships between quantile metrics from field- and lidar-derived vertical canopy profiles. Initially, complimentary metrics from both lidar and field profiles were compared. For example the correlation of the 75% metric for both lidar (CHP75 and HENG75) and field (FCV75) was examined using the metrics from all plots. Next, the mean difference for each metric was analyzed. This was calculated for each metric by subtracting the lidar metric (e.g., HENG25) from the corresponding field metric (FCV25), and then taking the mean of the differences for all plots. For example, if the mean of all FCV75-HENG75 values was a positive number then the lidar metric is “lower on average” than the corresponding field metric.

Next, we analyzed the relationship between the entire lidar- and field-derived vertical canopy profiles. The correlation of individual lidar and field profiles was examined for each plot. To do this, the untransformed lidar waveforms were converted into 180 (30-cm) bin profiles. Because the raw waveform bin size is 30 cm, this simply involved cutting the waveform at ground level and at 54 m (bin 180) above ground level. In addition, all untransformed lidar and field profiles were normalized to compensate for differences in units (i.e., crown area and digitizer counts). We initially examined the correlation of complete average lidar profiles and corresponding field profiles. However, whereas field profiles are only from the top of the highest canopy to the bottom of the lowest crown, lidar profiles are continuous from the canopy top to the ground. We, therefore, cut the portion of the lidar profile that was below the field-measured lowest live branch and reexamined the correlation between lidar and field profiles. Quantile metrics were not, however, recalculated for the cut lidar profiles.

As a final comparison of field and lidar profiles, we performed a goodness-of-fit analysis between lidar and field-based vertical canopy profiles. We measured the goodness-of-fit as the fraction of area shared by two types of normalized average profiles for each plot. The area overlap index (AOI) was calculated from the area of both average profiles that overlaps divided by the total area of both

profiles. Statistical significance of differences between lidar and field profiles was then assessed by randomization of subplot-level profiles (e.g., individual lidar footprints or crown volume distributions from 25-m diameter circular subsets within each plot). The normalized subplot-level profiles from lidar and field methods were first pooled together. Then AOI between the observed average vertical profiles were compared with AOI of average profiles from 999 pairs of subsets, composed of random partitions of subplot lidar and field data from within the same larger plot. If the “actual” AOI (i.e., between average lidar- and field-derived profiles) was less than all but 49 or fewer AOI from the randomization procedure, then the average profiles were considered significantly different ($\alpha=.05$)

Lastly, we identified the best linear combination of lidar profile metrics for predicting EAGB. Metrics from lidar profiles in all plots were used in a stepwise regression procedure to predict EAGB, and the best single and multiple-term relationships were identified. We then compared these relationships with corresponding relationships between EAGB and metrics from field profiles.

3. Results

3.1. Field-derived vertical canopy profiles

Nearly all of the metrics listed in Table 2 from field-derived vertical canopy profiles and the maximum and mean stem height increase from agroforestry to secondary forest, and from secondary to primary forest. The notable exception is for FCV05, which is higher in agroforestry plots than in secondary plots, but is still highest in primary forest plots. These trends are apparent in Fig. 4 where the narrow distribution of crown volume in the uniform agroforestry plots is all higher aboveground than the lower portion of canopy materials in the secondary (and in some cases primary) forest plots.

Table 2
Field characteristics by landcover type

Field variable	Agroforestry	Secondary	Primary
Number of plots	6	3	18
Max stem height (m)	10.4 (10.4–11.9)	34.6 (32.5–42.4)	40.0 (31.7–47.0)
Mean stem height (m)	9.4 (9.2–11.4)	14.3 (11.6–21.0)	16.9 (15.8–19.1)
FCV05 ^a (m)	7.0 (6.7–9.0)	6.0 (5.3–9.3)	8.0 (7.0–9.3)
FCV25 ^a (m)	7.6 (7.3–9.7)	12.0 (8.7–14.7)	12.3 (11.0–15.7)
HMFCV ^a (m)	8.4 (8.0–10.3)	16.7 (12.0–20.0)	16.9 (14.3–22.0)
FCV75 ^a (m)	9.2 (9.0–11.0)	20.7 (18.0–26.3)	22.7 (19.0–29.3)
FCV95 ^a (m)	9.7 (9.5–11.7)	25.0 (24.0–34.3)	31.7 (25.0–38.3)
EAGB (Mg/ha)	29 (28–48)	124 (70–193)	173 (113–206)

For field-derived vertical canopy profile metrics and field EAGB, the first value is the median and the values in parentheses are the range of values from all plots within each type.

^a Quantiles from field-estimated crown volume distribution (see Fig. 2 and text for details).

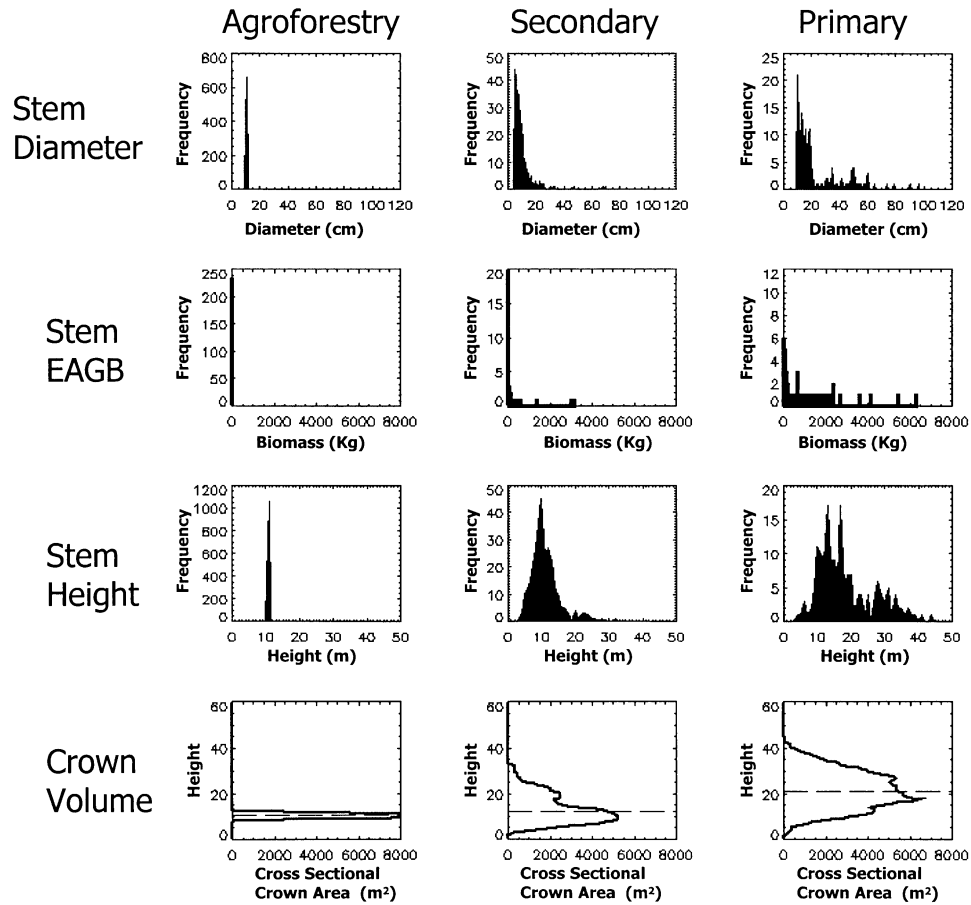


Fig. 4. Histograms of stem diameters, estimated stem biomass and stem height, and crown volume distributions from an example plot within three different landcover types. For crown volume distributions, the height of median crown volume (HMFCV) is represented by the dotted line.

3.2. Field-derived vertical canopy profile metrics vs. EAGB

The increase in most field profile metrics parallels an increase in EAGB from agroforestry to primary forest plots (Table 2). The range of EAGB varies greatly within secondary and primary forest plots. Within secondary plots large, remnant stems (i.e., those not cleared when the area was originally deforested) may comprise over 15% of the basal area in secondary forest areas (Guariguata et al., 1997) and, therefore, contribute a large proportion to the overall plot-level aboveground biomass. These remnant stems also

increase both height metrics (e.g., maximum height) and upper profile metrics (e.g., FCV95).

Table 3
Regression equations for field-estimated vertical canopy profile metrics vs. EAGB

Equation	R ²	RMSE (Mg/ha)
(1) $y = 6.2 \times \text{FCV95} - 28.5$.88	21.7
(2) $y = 3.9 \times \text{FCV99} + 15.9 \times \text{FCV10} - 126.6$.92	18.0
(3) $y = 7.7 \times \text{FCV99} + 20.2 \times \text{FCV10} - 5.71 \times \text{FCV90} - 141.7$.93	17.3
(4) $y = 7.6 \times \text{FCV99} + 46.0 \times \text{FCV10} - 7.2 \times \text{FCV90} - 24.6 \times \text{FCV05} - 144.7$.94	16.0

Data is from all plots (n = 26) sampled at La Selva Biological Station.

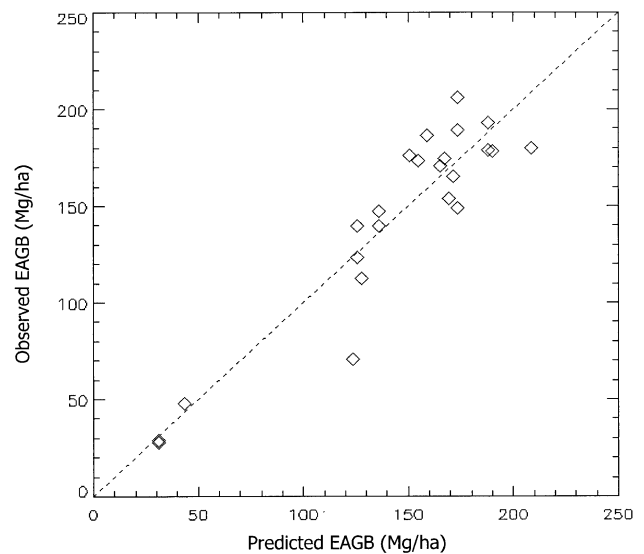


Fig. 5. Predicted vs. field EAGB from all plots at La Selva. The predicted EAGB values are from a single-term regression (Table 3, Eq. (1)) using the FCV95 metric from field-derived vertical canopy profiles.

Table 4
Lidar vertical canopy profile metrics by landcover type

Profile metric	Agroforestry	Secondary	Primary
HENG05 ^a (m)	− 1.7 (− 3.0–(− 1.3))	0.3 (− 1.8–1.3)	3.4 (− 1.2–7.1)
HENG25 ^a (m)	0.5 (− 1.5–3.8)	11.5 (4.7–11.7)	16.6 (9.9–21.2)
HOME ^a (m)	4.8 (0.3–7.4)	16.2 (9.0–17.6)	21.6 (12.0–28.4)
HENG75 ^a (m)	7.8 (2.1–9.7)	18.2 (14.0–25.5)	23.9 (19.6–33.7)
HENG95 ^a (m)	10.2 (5.7–12.8)	22.8 (20.6–34.5)	27.4 (24.6–37.5)
CHP05 ^b (m)	3.9 (3.0–4.4)	3.3 (3.1–3.9)	3.9 (2.5–6.1)
CHP25 ^b (m)	6.7 (4.3–8.0)	8.3 (7.3–8.5)	11.1 (8.2–14.1)
CHP50 ^b (m)	8.5 (5.3–10.4)	13.0 (11.1–14.0)	18.6 (13.7–23.9)
CHP75 ^b (m)	10.0 (6.7–12.3)	17.9 (15.4–22.1)	23.4 (18.3–31.1)
CHP95 ^b (m)	11.5 (8.0–13.1)	21.2 (21.0–28.5)	23.4 (18.3–37.1)

The first value is the median and the values in parentheses are the range of values from all plots within each landcover type.

^a Quantiles from untransformed waveforms (see Fig. 3 and text for details).

^b Quantiles from “canopy height profile” transformation of waveforms (see Fig. 3 and text for details).

As a result the best single predictor of EAGB ($R^2=.88$) across this wide range of conditions is a metric from the upper portion of the profiles, FCV95 (Table 3, Eq. (1)). The relationship between this field metric and EAGB is non-asymptotic across all land-use, successional and environmental conditions sampled at La Selva (Fig. 5). The standard error (RMSE) for this single-term relationship is 21.65 Mg/ha.

If two or more metrics were used in a multiple regression to predict differences in EAGB across all plots, the R^2 values increased further. With 4 metrics from the field vertical canopy profile, approximately 94% of the variation in EAGB was explained. In addition, the RMSE dropped to approximately 16 Mg/ha, which is approximately 10% of the mean EAGB value for primary forest plots at La Selva.

For the multiterm equations, the metrics that were the best predictors of EAGB (Table 3) were from both the upper and lower portions of the field profile (e.g., FCV90 and FCV10). Thus, differences in both the upper and lower portions of canopy profiles are highly related to variation in above-ground biomass in this neotropical landscape.

3.3. Lidar-derived vertical canopy profiles

In general, metrics from lidar vertical canopy profiles (waveforms and CHPs) also increase from agroforestry to secondary forest, and from secondary to primary forest (Table 4). As is the case for the field metric FCV05, the exception in this trend is the transformed lidar metric CHP05, which is higher in agroforestry and primary forest

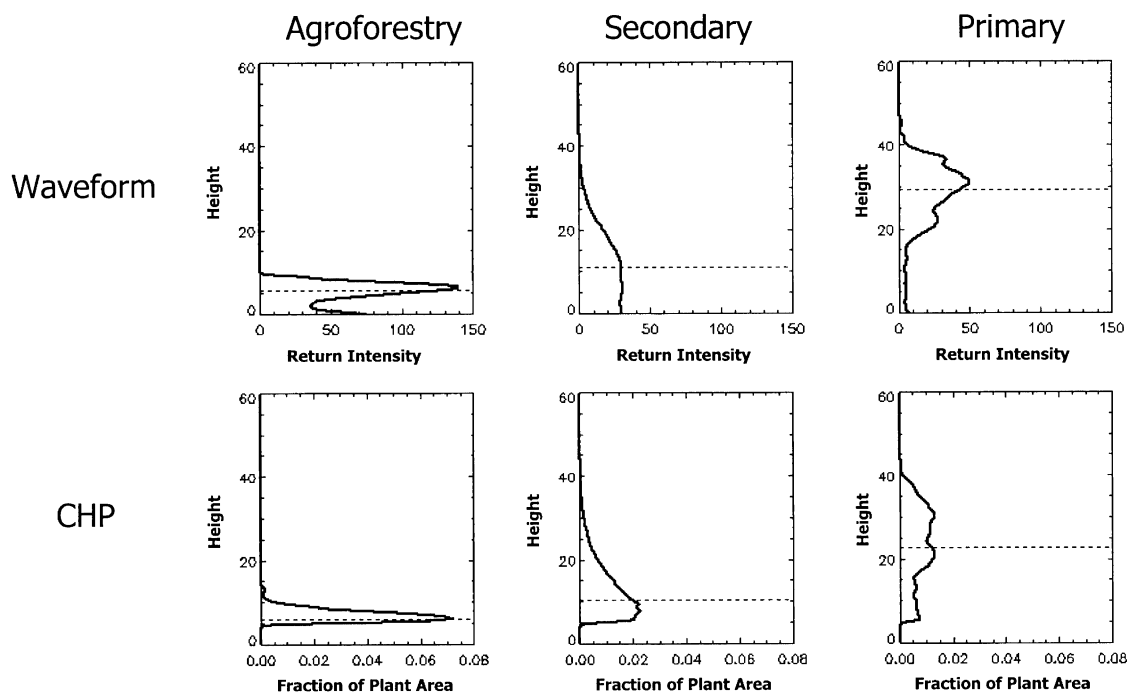


Fig. 6. Average lidar-derived vertical canopy profiles (waveforms and CHPs) from an example plot within three different landcover types. The median or 50% height for both the waveforms (HOME) and the CHP (CHP50) is represented by the dotted line.

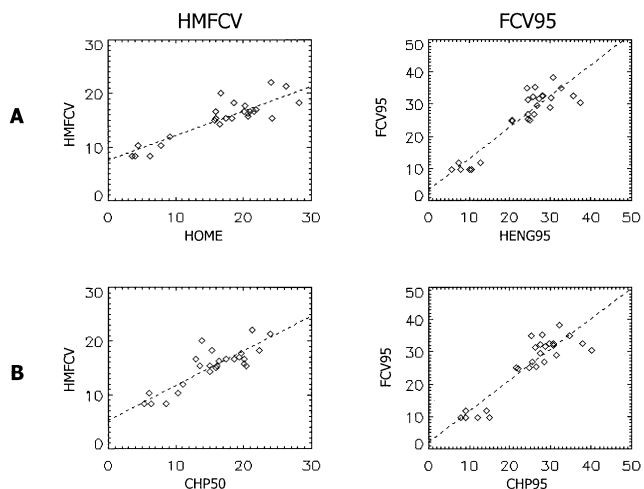


Fig. 7. Relationships between corresponding metrics derived from field (y-axis) and lidar (x-axis) vertical canopy profiles. (A) Relationships between two metrics from lidar waveforms (HOME, HENG95) and the corresponding field profile metrics (HMFCV, FCV95). (B) Relationships between two metrics from lidar CHPs (CHP50, CHP95) and the corresponding field profile metrics (HMFCV, FCV95). For all plots, the dotted line represents the regression line. See Table 5 for R^2 , RMSE, and mean difference values.

plots than in secondary plots. In contrast, the corresponding untransformed waveform metric, HENG05, does increase from agroforestry to primary forest. HENG05 is negative in several plots because the waveform is the entire lidar signal, including the ground return. In many cases (particularly in agroforestry plots), a large portion of the overall energy is in the lower portion of the last Gaussian pulse (i.e., below the ground reference level which is the peak of the last Gaussian pulse). These trends can be seen in Fig. 6 where there is an increase in the height of lidar profile metrics from agroforestry to primary forest plots.

3.4. Lidar- vs. Field-derived vertical canopy profile metrics

The values for most of the lidar vertical canopy profile metrics (Table 4) increase from agroforestry to primary forest plots and, therefore, follow a similar trend to the corresponding field metrics (Table 2). The values for upper metrics from both waveforms and CHPs closely mirror equivalent metrics in the field crown volume distributions (e.g., FCV95 vs. CHP95). In contrast, the differences

between the lower field and lidar quantiles (e.g., FCV05 vs. CHP05) are greater.

To further examine the relationship between corresponding lidar and field profile metrics, a simple linear regression analysis was performed. The regression results (Fig. 7, Table 5) illustrate that metrics from both lidar and field profiles are all highly correlated, except for the lower metrics (e.g., FCV05 vs. CHP05). In all but one case, the R^2 and RMSE values show the untransformed waveform metrics are more similar to the field profile metrics than the CHP metrics (Table 5A, Fig. 7). In most cases, the RMSE values on the waveform metric equations are less than 12% of the median value of the corresponding field metric, and are less than 14% of the median value in the CHP metric equations.

In most cases, the mean of differences between lidar and field metrics is less than 2 m (Table 5B). Again the exception is for the lowest profile metric where the mean difference is approximately 6 m for the waveform metric (FCV05-HENG05) and 4 m for the CHP metric (FCV05-CHP05). This illustrates that the bottom portion of the lidar profiles are typically lower than the field profiles. The most likely explanation for this it that the crown volume distributions start with the lowest branch on a measured tree (e.g., a tree over 10 cm dbh in primary plots). In contrast, lidar profiles are continuous from the top of the canopy to the ground (and below for waveforms as mentioned above). As a result, this difference is to be expected.

3.5. Lidar- vs. field-derived vertical canopy profiles

There is a fairly good qualitative agreement between lidar- and field-derived vertical canopy profiles (Fig. 8). Both average waveforms and average CHPs tend to follow a similar overall pattern as the field-derived vertical canopy profiles. With the exception of untransformed average waveforms in primary forest areas, lidar and field vertical canopy profiles tend to have their largest peaks at approximately the same height. In addition, the canopy heights (i.e., the top of the profile) from both lidar and field techniques are also closely related in all landcover types.

Lidar and field profiles in most plots are also highly correlated (Table 6). Waveforms and field profiles from secondary forest plots are the most highly correlated, followed by primary forest and agroforestry plots. In con-

Table 5 Comparison of corresponding metrics from field- and lidar-derived vertical canopy profiles

Lidar profile	FCV05	FCV25	HMFCV	FCV75	FCV95
<i>Regression results from field and associated lidar metrics (e.g., FCV25 vs. HENG25 or CHP25)</i>					
Waveform	0.22 (0.94 m)	0.78 (1.06 m)	0.81 (1.78 m)	0.79 (2.84 m)	0.83 (3.93 m)
CHP	0.01 (1.06 m)	0.53 (1.59 m)	0.74 (2.07 m)	0.80 (2.82 m)	0.80 (4.23 m)
<i>Mean difference values (field minus lidar) for each metric (m)</i>					
Waveform	6.07	- 0.33	- 1.12	- 0.21	1.62
CHP	4.10	1.81	- 0.15	- 0.20	0.95

R^2 and RMSE (parentheses) values are listed.

Table 6
Correlation between lidar- and field-based vertical canopy profiles

	Agroforestry	Secondary	Primary
<i>Correlation of lidar waveforms or CHP vs. crown volume distributions</i>			
Waveform	0.27 (0.06–0.70)	0.88 (0.79–0.93)	0.60 (0.02–0.85)
CHP	0.46 (0.01–0.78)	0.74 (0.57–0.90)	0.78 (0.45–0.93)
<i>Correlation using portion of lidar profiles that are above the lowest live crown measured in each plot</i>			
Waveform (Cut)	0.45 (0.05–0.86)	0.89 (0.83–0.93)	0.59 (0.07–0.87)
CHP (Cut)	0.62 (0.24–0.86)	0.74 (0.57–0.90)	0.80 (0.53–0.93)

For all comparisons, median correlation coefficients between lidar and field data for plots within each landcover type are listed first, followed by the observed range of coefficients in that type.

trast, CHPs and field profiles from primary forest plots are the most highly correlated, followed by secondary forest and agroforestry plots.

In both agroforestry and primary plots, CHPs are more highly correlated than waveforms with field-derived vertical canopy profiles. In secondary forest plots, however, untransformed waveforms were more highly correlated than CHPs with field profiles. This same general trend can be seen in Fig. 8, where removal of the ground return in agroforestry plots, and where transformation of the lower portion of the profile in primary forest plots allows the CHP to more closely resemble the field profiles. Similarly, because the field vertical canopy profiles are from the top of the canopy to the bottom of the lowest live crown for trees over 10-cm stem diameter (in primary plots), when the correlation analyses are only performed on the portion of both profiles within this range for each plot, there is a slight improvement in the correlations (Table 6B).

The results from goodness-of-fit analysis of lidar and field profiles follow similar trends (Table 7). The area of overlap between average waveform and field profiles (as

characterized by the AOI) is highest in secondary forests, followed by primary forests and agroforestry areas. The AOI between the average CHP and field profiles was greatest in primary forest plots, followed by secondary forest and agroforestry plots.

Although both correlation coefficients (Table 6) and AOI (Table 7) between lidar and field profiles are generally quite high, in most cases, the average profiles are significantly different (Table 7). In other words, the AOI between average lidar and field profiles for a given plot are typically smaller than the AOI from all 999 pairs of subsets composed of random partitions of subplot level field and lidar profiles. For example, in the agroforestry areas, lidar and field profiles in five out of six plots were significantly different. Similarly, average lidar profiles were significantly different from field profiles in 17 out of 18 primary forest plots. However, average waveforms were significantly different from field profiles in only one out of three secondary plots, whereas average CHPs were all significantly different from field profiles in secondary forest areas.

In summary, in many cases there are significant differences between profiles derived using lidar and field techniques. Nonetheless, the upper quantile metrics from lidar (e.g., HENG95 or CHP95) and field (e.g., FCV95) techniques are highly correlated. In addition, the mean differences between many of the upper metrics are less than 2 m. As such lidar data can resolve differences in canopy structure across this neotropical landscape, without equivalence to field profiles.

3.6. Lidar-derived vertical canopy profile metrics vs. EAGB

Metrics from lidar vertical canopy profiles follow a similar trend to metrics from field profiles: all lidar metrics except CHP05 (Table 4) are greater in plots with greater biomass (Table 2). As a result, lidar metrics are highly

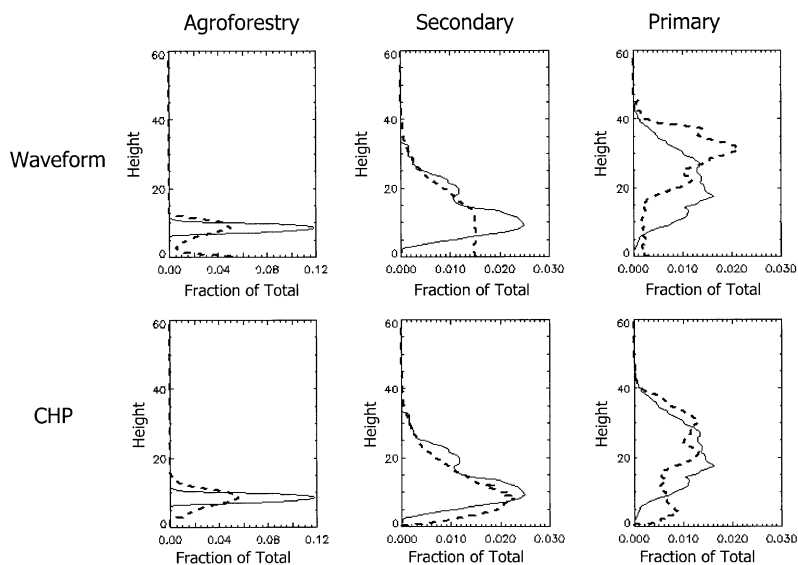


Fig. 8. Field and lidar (dashed line) vertical canopy profiles from an example plot within three different landcover types. All profiles have been normalized as a fraction of their total value (e.g., fraction of total crown volume).

Table 7

Goodness-of-fit between lidar- and field-based vertical canopy profiles measured as the fraction of area shared by two types of normalized average profiles for each plot

	Agroforestry	Secondary	Primary
Waveform	0.27 ^a (0.07–0.42)	0.82 ^b (0.77–0.86)	0.64 ^c (0.40–0.80)
CHP	0.38 ^a (0.20–0.48)	0.73 ^d (0.63–0.83)	0.75 ^c (0.59–0.86)

The AOI was calculated from the area of both average profiles that overlaps divided by the total area of both profiles. Statistical significance of differences between lidar and field profiles was assessed by randomization. Subplot data from field and lidar methods were pooled. Then AOI between the observed average vertical profiles were compared with AOI of average profiles from 999 pairs of subsets, composed of random partitions of subplot lidar and field data from within the same larger plot (see text). For all comparisons, median AOI between lidar and field data for plots within each landcover type are listed first, followed by the observed range of AOI values in that type.

^a Average profiles from one out of six plots were not significantly different ($P < .05$).

^b Average profiles from two out three plots were not significantly different ($P < .05$).

^c Average profiles from 1 out of 18 plots were not significantly different ($P < .05$).

^d Average profiles for all plots were significantly different ($P < .05$).

correlated with EAGB across all of the plots sampled (Table 8). The best single predictor of EAGB was the HOME metric with an R^2 value of .87 and an RMSE of approximately 23 Mg/ha (Table 8, Eq. (1)). Although this quantile metric differs from the best single predictor of EAGB from field profiles (i.e. FCV95), the level of variation that is explained by both metrics is approximately equal (88% vs. 87%, Tables 3 and 8). The relationship is also nonasymptotic across all land-use, successional and environmental conditions at La Selva (Fig. 9).

When two or more metrics are used in a multiple linear regression, the R^2 values increase (Table 8, Eqs. (2)–(4)), as with multiple regression results from field metrics. For example, with four metrics from the lidar profiles, the R^2 values are approximately .94, and the RMSE is approximately 16 Mg/ha (again, approximately 10% of the mean EAGB value for primary forest plots at La Selva). Another similarity with field equations is that the metrics that were the best predictors of EAGB were from both the upper and lower portions of the canopy (e.g., HENG10 and HENG90). However, one key difference between field and lidar equations is that the median metric (HOME) was in every lidar equation. Another important result is that for all equations, metrics from

Table 8

Regression equations for lidar vertical canopy profile metrics vs. EAGB

Equation	R^2	RMSE (Mg/ha)
(1) $y = 6.6 \times \text{HOME} - 24.8$.87	22.6
$y = 6.2 \times \text{HOME} - 0.75 \times \text{HENG10} + 26.5$.88	21.3
$y = 8.0 \times \text{HOME} + 8.4 \times \text{HENG10} - 9.8$ $\times \text{HENG25} + 64.4$.92	18.2
$y = 5.2 \times \text{HOME} + 10.5 \times \text{HENG10} - 12.5$ $\times \text{HENG25} - 3.6 \times \text{HENG90} + 49.8$.94	16.1

Data is from all plots ($n = 26$) sampled at La Selva Biological Station.

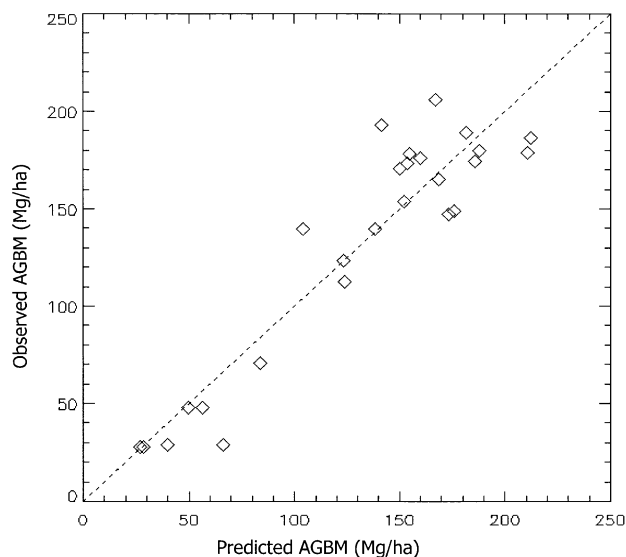


Fig. 9. Predicted vs. field EAGB from all plots at La Selva. The predicted EAGB values are from a single-term regression (Table 8, Eq. (1)) using the HOME metric from lidar-derived vertical canopy profiles.

the untransformed waveforms were chosen over CHP metrics through the stepwise multiple regression analysis.

4. Discussion

4.1. Relationship between field-derived vertical canopy profiles and biomass

The first portion of this research focused on the correlation between metrics from field-derived vertical canopy profiles and the total aboveground biomass. The strong relationship between single (e.g., FCV95) or multiple metrics from the field profiles and EAGB illustrates the value of quantifying variation in vertical canopy structure. The differences in the relative distribution of crown volume are strongly correlated with different EAGB levels across a wide variety of landcover types at La Selva Biological Station, including old-growth forest areas.

Some of the potential reasons that vertical canopy profiles are highly correlated with EAGB are illustrated in Fig. 4. Although the density of stems in agroforestry and secondary forest plots are much higher than in primary forest plots, it is the relatively few, very large canopy-forming individuals in primary forest plots that contribute heavily to the total aboveground biomass in each plot. In addition, these large individual stems constitute the bulk of the upper portion of the vertical canopy profiles in primary forest plots. In contrast, the relatively few remnant stems in secondary forest areas create only a small upper mode in both the vertical canopy profile and the distribution of stem heights (Fig. 4).

Similarly, within primary forest plots, the death of individual trees, and poor microenvironmental conditions can lead to lower-stature canopies (e.g., the low end of the

range for FCV95 in Table 2), with lower total EAGB (e.g., one primary forest plot had an EAGB of only 113 Mg/ha, Table 2). As a result, upper quantile metrics (e.g. FCV95) from the field-derived vertical canopy profiles are highly correlated with overall EAGB across this landscape.

The relationship between metrics from field-derived vertical canopy profiles and aboveground biomass is important because it illustrates that height and canopy structure are important indicators of current ecosystem state. More importantly, metrics that relate to differences in the relative vertical distribution of canopy structure are responsive to variation in total aboveground biomass across the entire range of conditions sampled. It is reasonable that vertical canopy structure should be correlated to aboveground biomass in forest ecosystems, however, the relationship between canopy metrics (e.g., crown volume metrics) and aboveground biomass is not well established for most forests. Most field studies have instead focused on the relationship between the height and biomass of individual stems, and not the relationship between vertical canopy structure and biomass at a plot (e.g., 0.5 ha) level. Because lidar instruments are sensitive to variation in canopy structure in a variety of forests (Harding et al., 2001; Lefsky, Cohen et al., 1999), there is a need to examine the relationships between canopy structure and aboveground biomass from a field perspective as well. Our results suggest that differences in the relative vertical distribution of canopy structure provide an important means to characterize the current state of neotropical ecosystems.

4.2. Relationship between complete field- and lidar-derived vertical canopy profiles

We have demonstrated that metrics from field-derived canopy profiles are correlated with EAGB at La Selva. Next, we examined the sensitivity of lidar data to differences in canopy structure across different landcover types (e.g., agroforestry, secondary and primary forest). Although field and lidar profiles are correlated and have high AOI (Tables 6 and 7, respectively), in many cases, there are significant differences between field and lidar profiles on a plot-to-plot basis (Table 7, Fig. 8). Similarly, Harding et al. (2001) also found that lidar CHPs and field profiles (derived from ground-based sightings to plant intercepts) had qualitative similarities but were statistically different.

To a certain degree, the differences between entire profiles from lidar and field techniques found in this study should be expected. The effects of modeling stem heights and crown dimensions (Table 1) for many stems, as well as the assumption that crowns are filled cylinders are simplifications. In reality, crowns are highly irregular in shape, and crown materials are often clumped. Whether these model assumptions lead to biases in the field profiles in relation to the true distribution of crown volume is uncertain. However, they will certainly contribute to differences between field and lidar profiles.

Even if the forest structure in each plot were destructively sampled to provide an actual crown volume distribution, there would still likely be differences between these profiles and lidar profiles. First, lidar instruments sample the entire distribution of canopy materials from the highest crown to the ground, whereas the field profiles developed in this study are only from the highest crown to the base of the lowest crown sampled. Second, trees that were used to create the crown volume distribution were only a portion of the plants that are found in each plot. Trees that were under 10 cm diameter (5 cm in secondary plots) were not included. As a result, the field profiles do not include many of the smaller trees that also contribute to the lidar profiles.

A third cause for differences between lidar and field profiles is that the lidar signal is affected by the decreasing total amount of energy as the pulse travels lower into the canopy. For example, in Fig. 8, the upper portion of the lidar waveform is higher than the corresponding field-derived profile in a primary forest plot. Although a modified MacArthur–Horn transformation of the signal may make intuitive sense to compensate for this problem, there are still important assumptions (e.g., horizontal homogeneity or no clumping of canopy materials) that may create other biases (Harding et al., 2001; Lefsky, Cohen et al., 1999; Means et al., 1999). In this case, the transformation of the waveforms into CHPs did increase the correlation and goodness-of-fit values (Tables 6 and 7) with field profiles in primary forest and agroforestry areas compared with the untransformed waveforms, but there were still the same number of significant differences between field and lidar profiles. The correlation and goodness-of-fit of CHP and field profiles in secondary forest areas were lower than the untransformed waveform values. Further, all of the secondary forest plots had significant differences after the transformation, whereas the average waveform and field profiles from two of the three secondary forest plot areas were not significantly different. Thus, it is unclear if the modified MacArthur–Horn transformation of the lidar signal improves representation of canopy structure in this neotropical landscape.

Although significant differences exist between lidar and field profiles, there are also important qualitative similarities (Fig. 8). For example, both lidar and field profiles from different landcover types are distinct. To test if lidar data are sensitive to differences in canopy structure between different landcover types, we performed an additional goodness-of-fit analysis where we compared “type-level” average waveforms or CHPs produced from all individual waveforms or CHPs in one landcover type (e.g., primary forest) with the corresponding type-level profile from another landcover type (e.g., secondary forest). To test for significance, we compared the AOI from these type level comparisons with the AOI from 999 pairs of subsets where all individual profiles (i.e., CHP or waveforms) from both landcover types were first pooled and then were randomly partitioned to create new “synthetic type-level” profiles. In all cases, the lidar profiles from each landcover type were significantly different ($P < .005$) from

all other landcover types. This shows that large-footprint lidar instruments are sensitive to important differences in vertical canopy structure in this neotropical forest and can, thus, be used to differentiate landcover types.

4.3. Relationship between metrics from field- and lidar-derived vertical canopy profiles

Although significant differences exist between the complete normalized vertical canopy profiles from lidar and field techniques, metrics from both field and lidar profiles are highly correlated (Table 5), and the mean differences between corresponding upper quantile metrics (e.g., FCV95 vs. HENG95) are all small (<2 m). This demonstrates that lidar is sensitive to important differences in canopy structure both within and across landcover types.

Comparisons of the quantile metrics derived from lidar and field profiles are not as strongly influenced by subtle differences in the overall spread of the profiles as are goodness-of-fit comparisons of the complete profiles. As such, although there are obvious differences in the bottom-most metrics (e.g., FCV05 vs. HENG05, Table 5), the upper metrics from both lidar and field profiles are closely related. This is important because upper quantile metrics from the field profiles (FCV95) were the best predictors of EAGB in this neotropical landscape.

4.4. Comparison of the relationships between field- and lidar-derived vertical canopy profiles and biomass

We found that metrics from lidar vertical canopy profiles are approximately as correlated with EAGB (Table 8) at La Selva as field profile metrics (Table 3). This shows that large-footprint lidar instruments are sensitive to variation in EAGB, despite the significant differences between some lidar and field profiles.

In a related study (Drake et al., 2002), we found that mean canopy height and the HOME from lidar waveforms were highly correlated with EAGB at La Selva. This extension of that earlier work provides a more thorough examination of the relationship between the complete lidar profile and EAGB, and also allows for a comparison with similar field techniques.

Although the best single predictor of EAGB from field (FCV95) and lidar (HOME) profiles differs, if the corresponding lidar metric is used instead (i.e., HENG95) the relationship is still quite strong ($R^2=0.83$). The HOME metric may be more strongly influenced by the amount of lidar energy that penetrates to the ground and, therefore, will be much lower in areas with more open canopy conditions. For example in the agroforestry areas HOME is much lower than HENG95 (Table 4, Fig. 6) caused primarily by the presence of strong ground returns. This may help to explain why metrics from untransformed waveforms were selected over CHP metrics in a stepwise multiple regression analysis (Table 8). Because the ground return is redistributed to the

canopy return during the modified MacArthur–Horn technique (Harding et al., 2001), these metrics may not be sensitive to differences in both canopy structure and openness in different landcover types. In any case, waveform transformation did not improve estimates of biomass.

5. Conclusions

Although past research has examined changes in field-derived vertical canopy profiles (e.g., foliar height profiles) through different stages of forest succession (Aber, 1979a, 1979b; Brown & Parker, 1994; Paré & Bergeron, 1995), the relationship between metrics from field profiles and biomass has generally not been examined, primarily because vertical canopy profiles are difficult to construct. Because large-footprint lidar instruments can rapidly record vertical canopy profiles over large forested areas in contrast to labor-intensive field methods, they represent a breakthrough in the remote sensing of forest canopy structure with great potential for large-scale land surface characterization.

In this study, we found that lidar data are sensitive to important differences in canopy structure over a wide range of conditions (i.e., from young secondary forests to primary tropical rainforests). We also showed that lidar profiles (even with a MacArthur–Horn transformation) are not equivalent to field profiles of the vertical distribution of crown volume. Nonetheless, metrics from untransformed lidar profiles are as good as metrics derived from field profiles for biomass estimation. Because changes in canopy structure are highly correlated with changes in aboveground biomass through time, lidar provides a new method for estimating carbon stocks in dense tropical forests.

The remaining challenge is to explore the generality of the relationships between vertical canopy profiles and aboveground biomass in different forest ecosystems. For example, will the relationships developed at La Selva Biological Station, a tropical wet forest (Holdridge et al., 1971) also apply to tropical moist forests in the Amazon that may receive half of the La Selva rainfall totals? Our future work will test the generality of these relationships in other tropical regions and will develop new relationships in areas with different environmental conditions if necessary. This process will set the stage for using global lidar observations from future spaceborne lidar instruments, such as the VCL (Dubayah et al., 1997), to estimate biomass in terrestrial ecosystems globally.

Acknowledgments

We thank David Rabine who helped operate LVIS. Michelle Hofton, Nancy Casey-McCabe, and Dave Kendig for their help in processing the LVIS data, and Robin Chazdon for the use of her secondary forest field data.

We are grateful to Leonel Campos Ramos, William Conejo Miranda, Marcos Molina, Jeanette Paniagua, Braulio Vilchez, Robin Chazdon, Laura Rochio, Birgit Peterson, Steve Prince, and John Weishampel for valuable help in collecting field data. Our special thanks also go to the La Selva Biological Station, the Organization for Tropical Studies, the Carbono Project (funded by DOE, NSF and the Andrew W. Mellon Foundation), the Wallops Flight Facility Aircraft Programs Office, the National Geographic Institute of Costa Rica, and the Government of Costa Rica. Our project is funded by a NASA contract to the University of Maryland for the implementation and execution of the VCL Mission under the Earth System Science Pathfinder program. In addition, J. Drake is funded through a NASA Earth System Science Fellowship.

References

- Aber, J. D. (1979a). Foliage-height profiles and succession in Northern hardwood forests. *Ecology*, *60*, 18–23.
- Aber, J. D. (1979b). A method for estimating foliage-height profiles in broad-leaved forests. *Journal of Ecology*, *67*, 35–40.
- Blair, J. B., & Hofton, M. A. (1999). Modeling laser altimeter return waveforms over complex vegetation using high-resolution elevation data. *Geophysical Research Letters*, *26*, 2509–2512.
- Blair, J. B., Rabine, D. L., & Hofton, M. A. (1999). The Laser Vegetation Imaging Sensor (LVIS): a medium-altitude, digitization-only, airborne laser altimeter for mapping vegetation and topography. *ISPRS Journal of Photogrammetry and Remote Sensing*, *54*, 115–122.
- Brown, M. J., & Parker, G. G. (1994). Canopy light transmittance in a chronosequence of mixed-species deciduous forests. *Canadian Journal of Forest Research*, *24*, 1694–1703.
- Brown, S. (1997). Estimating biomass and biomass change of tropical forests: a primer. *UN-FAO Forestry Paper 134*. Rome, Italy.
- Chazdon, R. L. (1996). Spatial heterogeneity in tropical forest structure: canopy palms as landscape mosaics. *Trends in Ecology and Evolution*, *11*, 8–9.
- Clark, D. B., & Clark, D. A. (2000). Landscape-scale variation in forest structure and biomass in a tropical rain forest. *Forest Ecology and Management*, *137*, 185–198.
- Curran, P. J., Foody, G. M., Lucas, R. M., Honzak, M., & Grace, J. (1997). The carbon balance of tropical forests: from the local to the regional scale. In: P. R. van Gardingen, G. M. Foody, & P. J. Curran (Eds.), *Scaling-up from call to landscape* (pp. 201–227). Cambridge: Cambridge University Press.
- Dixon, R. K., Brown, S., Houghton, R. A., Solomon, A. M., Trexler, M. C., & Wisniewski, J. (1994). Carbon pools and flux of global forest ecosystems. *Science*, *263*, 185–190.
- Drake, J. B., Dubayah, R. O., Clark, D. B., Knox, R. G., Blair, J. B., Hofton, M. A., Chazdon, R. L., Weishampel, J. F., & Prince, S. (2002). Estimation of Tropical Forest Structural Characteristics Using Large-footprint Lidar. *Remote Sensing of Environment*, *79*, 305–319.
- Drake, J. B., & Weishampel, J. F. (2000). Multifractal analysis of canopy height measures in a longleaf pine savanna. *Forest Ecology and Management*, *128*, 121–127.
- Dubayah, R., Blair, J. B., Bufton, J. L., Clark, D. B., JaJa, J., Knox, R. G., Luthcke, S. B., Prince, S., & Weishampel, J. F. (1997). The vegetation canopy lidar mission. *Land satellite information in the next decade: II. Sources and applications* (pp. 100–112). Bethesda, MD: American Society for Photogrammetry and Remote Sensing.
- Dubayah, R. O., & Drake, J. B. (2000). Lidar remote sensing for forestry. *Journal of Forestry*, *98*, 44–46.
- Dubayah, R. O., Knox, R. G., Hofton, M. A., Blair, J. B., & Drake, J. B. (2000). Land surface characterization using lidar remote sensing. In: M. J. Hill, & R. J. Aspinall (Eds.), *Spatial information for land use management* (pp. 25–38). Australia: Gordon & Breach Science Publishers.
- Foody, G. M., Palubinskas, G., Lucas, R. M., Curran, P. J., & Honzak, M. (1996). Identifying terrestrial carbon sinks: classification of successional stages in regenerating tropical forest from Landsat TM data. *Remote Sensing of Environment*, *55*, 205–216.
- Guariguata, M. R., Chazdon, R. L., Denslow, J. S., Dupuy, J. M., & Anderson, L. (1997). Structure and floristics of secondary and old-growth forest stands in lowland Costa Rica. *Plant Ecology*, *132*, 107–120.
- Harding, D. J., Lefsky, M. A., Parker, G. G., & Blair, J. B. (2001). Laser altimeter canopy height profiles: methods and validation for closed-canopy, broadleaf forests. *Remote Sensing of Environment*, *76*, 283–297.
- Holdridge, L. R., Grenke, W. C., Hatheway, W. H., Liang, T., & Tosi, J. A. J. (1971). *Forest environments in tropical life zones: a pilot study*. New York, NY: Pergamon.
- Imhoff, M. L. (1995). Radar backscatter and biomass saturation—ramifications for global biomass inventory. *IEEE Transactions On Geoscience and Remote Sensing*, *33*, 511–518.
- Lefsky, M. A. (1997). Application of lidar remote sensing to the estimation of forest canopy and stand structure. Ph.D. dissertation. Department of Environmental Sciences, University of Virginia, Charlottesville. p. 185.
- Lefsky, M. A., Cohen, W. B., Acker, S. A., Parker, G. G., Spies, T. A., & Harding, D. (1999a). Lidar remote sensing of the canopy structure and biophysical properties of Douglas-fir western hemlock forests. *Remote Sensing of Environment*, *70*, 339–361.
- Lefsky, M. A., Harding, D., Cohen, W. B., Parker, G., & Shugart, H. H. (1999b). Surface lidar remote sensing of basal area and biomass in deciduous forests of eastern Maryland, USA. *Remote Sensing of Environment*, *67*, 83–98.
- Luckman, A., Baker, J., Kuplich, T. M., Yanasse, C. D. F., & Frery, A. C. (1997). A study of the relationship between radar backscatter and regenerating tropical forest biomass for spaceborne SAR instruments. *Remote Sensing of Environment*, *60*, 1–13.
- MacArthur, R. H., & Horn, H. S. (1969). Foliage profile by vertical measurements. *Ecology*, *50*, 802–804.
- Magnussen, S., Eggermont, P., & LaRiccia, V. N. (1999). Recovering tree heights from airborne laser scanner data. *Forest Science*, *45*, 407–422.
- Matlock Jr., R. B., & Hartshorn, G. S. (1999). Organization for tropical studies: La Selva Biological Station. *Bulletin of the Ecological Society of America*, *80*, 188–193.
- McDade, L. A., Bawa, K. S., Hespeneide, H. A., & Hartshorn, G. S. (Eds.) (1994). *La Selva: ecology and natural history of a neotropical rain forest*. Chicago: University of Chicago Press.
- Means, J. E., Acker, S. A., Harding, D. J., Blair, J. B., Lefsky, M. A., Cohen, W. B., Harmon, M. E., & McKee, W. A. (1999). Use of large-footprint scanning airborne lidar to estimate forest stand characteristics in the Western Cascades of Oregon. *Remote Sensing of Environment*, *67*, 298–308.
- Menalled, F. D., Kelty, M. J., & Ewel, J. J. (1998). Canopy development in tropical tree plantations: a comparison of species mixtures and monocultures. *Forest Ecology and Management*, *104*, 249–263.
- Moran, E. F., Brondizio, E., Mausel, P., & Wu, Y. (1994). Integrating Amazonian vegetation, land-use, and satellite data. *Bioscience*, *44*, 329–338.
- Nelson, R., Swift, R., & Krabill, W. (1988). Using airborne lasers to estimate forest canopy and stand characteristics. *Journal of Forestry*, *86*, 31–38.
- Nicotra, A. B., Chazdon, R. L., & Iriarte, S. V. B. (1999). Spatial heterogeneity of light and woody seedling regeneration in tropical wet forests. *Ecology*, *80*, 1908–1926.
- Niklas, K. J. (1994). *Plant allometry: the scaling of form and process*. Chicago, IL: University of Chicago Press.

- Paré, D., & Bergeron, Y. (1995). Above-ground biomass accumulation along a 230-year chronosequence in the southern portion of the Canadian boreal forest. *Journal of Ecology*, 83, 1001–1007.
- Parker, G. G., Lefsky, M. A., & Harding, D. J. (2001). Light transmittance in forest canopies determined using airborne lidar altimetry and in-canopy quantum measurements. *Remote Sensing of Environment*, 76, 298–309.
- Peterson, B. E. (2000). *Recovery of forest canopy heights using large-footprint lidar*. MA thesis, Department of Geography, University of Maryland, College Park, 58 pp.
- Pierce, S. (1992). *La Selva Biological Station history: colonization/landuse/deforestation of Sarapiquí, Costa Rica*. MS thesis, Colorado State University, Fort Collins, CO.
- Sader, S. A., Waide, R. B., Lawrence, W. T., & Joyce, A. T. (1989). Tropical forest biomass and successional age class relationships to a vegetation index derived from Landsat TM data. *Remote Sensing of Environment*, 28, 143–156.
- Steininger, M. K. (2000). Satellite estimation of tropical secondary forest above-ground biomass: data from Brazil and Bolivia. *International Journal of Remote Sensing*, 21, 1139–1157.
- Strahler, A. H. (1997). Vegetation canopy reflectance modeling—recent developments and remote sensing perspectives. *Remote Sensing Reviews*, 15, 179–194.
- Waring, R. H., Way, J. B., Hunt, E. R., Morrissey, L., Ranson, K. J., Weishampel, J. F., Oren, R., & Franklin, S. E. (1995). Biologists toolbox—imaging radar for ecosystem studies. *Bioscience*, 45, 715–723.
- Weishampel, J. F., Ranson, K. J., & Harding, D. J. (1996). Remote sensing of forest canopies. *Selbyana*, 17, 6–14.
- Wickland, D. E. (1991). Global ecology: the role of remote sensing. In: G. Esser, & D. Overdieck (Eds.), *Modern ecology, basic and applied aspects* (pp. 723–750). New York, NY: Elsevier.